

## Viscous fingering in liquid crystals

A. Buka,\* P. Palffy-Muhoray,<sup>†</sup> and Z. Rácz<sup>‡</sup>

*Department of Physics, The University of British Columbia, Vancouver, British Columbia, Canada V6T 2A6*

(Received 16 March 1987)

We have studied the Saffman-Taylor instability in a Hele-Shaw cell containing the nematic liquid crystal 4,4'-*n*-octylcyanobiphenyl (8CB). Air injected into the center of the cell gives rise to viscous fingering patterns, which show a sequence of dense-branching, dendritic, dense-branching morphologies as a function of temperature. A qualitative explanation of these morphological transitions is given in terms of the flow alignment of the director field and the resulting anisotropic viscosity in the nematic phase of the liquid crystal. The fingering patterns were digitized; analysis of the resulting data shows that while the perimeter of the pattern is fractal, the pattern itself is not. The extent to which the pattern is space filling depends on the morphology and this quantity may serve to indicate the morphological transitions.

### INTRODUCTION

Much interest has been displayed recently in the structure of the interfacial patterns obtained when a low-viscosity fluid displaces a high-viscosity one in a Hele-Shaw cell. The typically ramified fingering patterns arise from a competition between surface tension and the instability due to the viscosity difference of the two liquids. The role of anisotropy in determining the morphology of these interfacial patterns is a question of fundamental importance. In this paper we report the results of experiments on a liquid crystal system demonstrating the effects of anisotropy on interfacial pattern selection.

Systems consisting of isotropic fluids have been studied experimentally.<sup>1-3</sup> In general, the patterns obtained are characterized by tip splitting and belong to the non-fractal dense-branching morphology.<sup>4</sup> In the limit of vanishing interfacial energy between the two fluids, the patterns are similar to the fractal morphology encountered in diffusion-limited aggregation.<sup>3,5</sup> In the presence of anisotropy, the tips of the viscous fingers may become stabilized, and dendritic patterns can then be observed.<sup>6</sup> In the case of isotropic fluids, the anisotropy has been introduced by engraving a grid on one of the plates of the Hele-Shaw cell.<sup>6</sup> Similar results have been observed in computer simulations where the anisotropy has been introduced by means of a lattice consisting of two types of lattice sites.<sup>5</sup>

Liquid crystals are fluids which undergo a transition from the isotropic liquid to other more ordered liquid phases. These phases are characterized by temperature-dependent anisotropic bulk properties. A two-fluid system consisting of a liquid crystal and air might therefore be expected to show dendritic behavior with stable tip growth for some range of control parameters. This behavior has already been observed in a nematic mixture at constant temperature.<sup>7</sup>

This paper reports results obtained on a Hele-Shaw cell containing a thermotropic liquid crystal which exhibits isotropic (*I*), nematic (*N*), and smectic *A* (*S<sub>A</sub>*) phases. Since the viscosity coefficients are temperature dependent, it is possible to control the anisotropy re-

sponsible for morphological transitions by controlling the temperature.

### THEORETICAL CONSIDERATIONS

In this section we consider a Hele-Shaw cell with the circular Paterson geometry<sup>8</sup> filled with a liquid crystal into which air is injected under pressure. We assume that viscous effects dominate and that inertial terms can be neglected. If the velocity profile of the viscous liquid between the parallel plates of the cell is parabolic, then the average velocity  $\bar{V}$  of the flow in the isotropic fluid phase of the liquid crystal is given by<sup>9</sup>

$$\bar{V} = -\frac{b^2}{12\mu} \nabla P, \quad (1)$$

where  $b$  is the separation between the plates,  $\mu$  is the viscosity, and  $P$  is the pressure. Since the divergence of the velocity field in an incompressible fluid is zero,

$$\nabla^2 P = 0. \quad (2)$$

The pressure field, therefore, satisfies Laplace's equation subject to boundary conditions on the interface. These boundary conditions are the following.

(a) The excess pressure of the injected air at the interface is constant,  $P_0$ .

(b) There is a pressure drop  $\sigma/R$  across the interface, where  $\sigma$  is the surface tension and  $R$  is the radius of curvature of the interface in the plane of the cell.

(c) There is a kinetic term, causing an additional pressure drop across the moving interface equal to  $7.6\mu^{2/3}V^{2/3}\sigma^{1/3}/b$  due to the effect of the wetting of the cell walls by the displaced fluid.<sup>4,10,11</sup> Here  $V$  is the normal velocity of the interface. These give an expression for the pressure on the viscous fluid side of the interface

$$P = P_0 - \frac{\sigma}{R} - \frac{7.6\mu^{2/3}V^{2/3}\sigma^{1/3}}{b}.$$

Once the pressure field is known, the velocity and hence the time evolution of the interface can be obtained from Eq. (1). The interface is perturbed by random fluctuations. The stability of the interface against these pertur-

bations may be examined heuristically as follows.

A perturbation of wavelength  $\lambda$  on the stationary interface decays with velocity<sup>12</sup>

$$V_p \approx \frac{4b^2\sigma}{\mu\lambda^2};$$

this is independent of the amplitude of the perturbation if the perturbation is small. If the interface is moving with velocity  $V$ , then perturbations whose speed  $V_p$  is greater than  $V$  will decay, while those whose speed is smaller will grow. For a circular interface of radius  $R$ , the pressure in the viscous fluid at a distance  $r$  ( $r \geq R$ ) from the center is

$$P = \left[ P_0 - \frac{\sigma}{R} \right] \frac{\ln(r/R_0)}{\ln(R/R_0)}, \quad (3)$$

where  $R_0$  is the cell radius, and the kinetic term in the boundary condition has been neglected. The velocity with which the interface propagates is therefore

$$V = \frac{b^2}{12\mu} \left[ P_0 - \frac{\sigma}{R} \right] \frac{1}{R \ln(R_0/R)}.$$

On this interface, only perturbations with wavelength greater than a critical value  $\lambda_c$  given by

$$\lambda_c = 2b \left[ \frac{\sigma}{\mu V} \right]^{1/2}$$

will grow. An approximately semicircular tip will therefore be stable if

$$\frac{\lambda_c}{R} = \left[ \frac{48 \ln(R_0/R)}{P_0 R / \sigma - 1} \right]^{1/2} > 1. \quad (4)$$

A circular interface with a small radius of curvature will therefore be stable, and will grow, increasing the radius of curvature until  $\lambda_c/R \approx 1$  and the tip becomes unstable. The tip then splits, the radii of curvature are reduced to stable values, and the process is repeated.

A more rigorous linear stability analysis, including the kinetic term, can be constructed by generalizing the approach of Mullins and Sekerka.<sup>13</sup> We consider a nearly circular interface of radius  $R_s$  in polar coordinates at time  $t=0$  given by

$$R_s = R(1 + \epsilon_m \cos m\theta),$$

where  $\epsilon_m$  is the relative amplitude of a small perturbation with wave number  $m$ . Solving Laplace's equation to order  $\epsilon_m$  subject to the boundary conditions on this interface and calculating the interface velocity gives the time evolution of the perturbation<sup>10</sup>

$$\frac{\dot{\epsilon}_m/\epsilon_m}{\dot{R}/R} = -2 + \frac{m \left[ 1 + \frac{2}{3}\bar{\beta} - \frac{m^2-1}{RP_0/\sigma-1} [\ln(R_0/R) + \bar{\beta}] \right]}{\frac{2}{3}m\bar{\beta} + \frac{R_0^{2m} - R^{2m}}{R_0^{2m} + R^{2m}}}, \quad (5)$$

where

$$\bar{\beta} = \frac{v}{1-v} \ln(R_0/R)$$

and

$$\frac{v^{3/2}}{1-v} = \frac{7.6^{3/2}}{12} \left[ \frac{P_0 b}{\sigma} - \frac{b}{r} \right]^{-1/2} \frac{b}{R \ln(R_0/R)}.$$

A similar result has been obtained by Ben-Jacob *et al.*<sup>4</sup> who assumed the kinetic term to be linear in the velocity of the interface.

The interface will be stable against fluctuations of wave number  $m$  if the right-hand side of Eq. (5) is negative. Again, we find that for small  $R$  the tip is stable. Ignoring the kinetic term ( $\beta=0$ ), the stability condition becomes

$$\frac{\ln(R_0/R)}{P_0 R / \sigma - 1} > \frac{1}{m^2 - 1} \left[ 1 - \frac{2}{m} \right].$$

For a semicircular tip, we expect the least value of  $m$  leading to an observable instability to be  $m \approx 4$ ; this result thus agrees with the heuristic argument above.

For a given unstable tip, the wave number  $m^*$  of the fastest-growing perturbation is the value of  $m$  which maximizes<sup>10</sup> the right-hand side of Eq. (5). Again, if kinetic terms are neglected,

$$m^* = \left[ \frac{1}{3} \left( \frac{P_0 R / \sigma - 1}{\ln(R_0/R)} + 1 \right) \right]^{1/2}. \quad (6)$$

The predictions of linear stability theory can therefore be tested by comparing the experimentally determined number of fingers initially appearing on a circular interface. This has been carried out;<sup>10</sup> very good agreement between experimental results and theory has been found.

Liquid crystals are fluids with anisotropic bulk properties resulting from long-range orientational order of the constituent molecules. Nematics exhibit cylindrical symmetry in second rank tensor properties, where the symmetry axis is the director  $\hat{n}$ . The flow properties of nematics are similar to other isotropic organic liquids consisting of molecules of similar size, though the flow regimes are more complex for the following reason: in a nematic, the translational motion is coupled to the orientational motion of the molecules. The velocity  $\bar{V}$  will influence the alignment and, conversely, a change in the

alignment can induce a flow in the nematic. This behavior has been described in the hydrodynamic theory of Ericksen<sup>14</sup> and Leslie<sup>15</sup> which involves five independent viscosity coefficients.

In the case of simple two-dimensional shear flow between two parallel plates, the viscous torque density  $\Gamma_x$  exerted on the molecules is<sup>16</sup>

$$\Gamma_x = [\alpha_2 \sin^2 \Theta(z) - \alpha_3 \cos^2 \Theta(z)] \frac{\partial V}{\partial z}, \quad (7)$$

where

$$\vec{V} = (0, V_y(z), 0),$$

$$\hat{n} = (0, \cos \Theta, \sin \Theta),$$

the plates are parallel to the  $x$ - $y$  plane, and  $\alpha_2$  and  $\alpha_3$  are shear viscosities.

For a typical nematic, both  $\alpha_2$  and  $\alpha_3$  are negative and  $\alpha_3/\alpha_2 < 1$ ; consequently, there exists an equilibrium angle  $\Theta_0$  between  $\hat{n}$  and  $\vec{V}$ , for which  $\Gamma_x$  vanishes, given by

$$\tan^2 \Theta_0 = \alpha_3 / \alpha_2. \quad (8)$$

In the above geometry a nematic director under shear tends to be aligned in the  $(z$ - $y)$  plane with an angle  $\Theta_0$  to the flow velocity.  $\Theta_0$  and its temperature dependence can be determined from birefringence measurements.<sup>17</sup>

### EXPERIMENTAL

Two parallel glass plates without surface treatment were used to construct the Hele-Shaw cell. The cell dimensions were 120 mm  $\times$  120 mm; the plates were separated by 30- $\mu$ m Mylar spacers at the corners. The cell was filled with liquid crystal, and air was injected through a hole in the center of one of the plates. The liquid crystal used in the experiment was 8CB (4,4'-*n*-octylcyanobiphenyl) with a phase sequence:

$$\text{isotropic} \xrightarrow{40.5^\circ\text{C}} \text{nematic} \xrightarrow{32.5^\circ\text{C}} \text{smectic } A.$$

In order to achieve patterns with a higher contrast, the liquid crystal was colored by adding 1.2 wt. % of the blue dye D27 from BDH Chemicals Ltd.

Air was injected into the cell at essentially constant pressure,  $P_0 = 0.06$  atm. The temperature of the sample

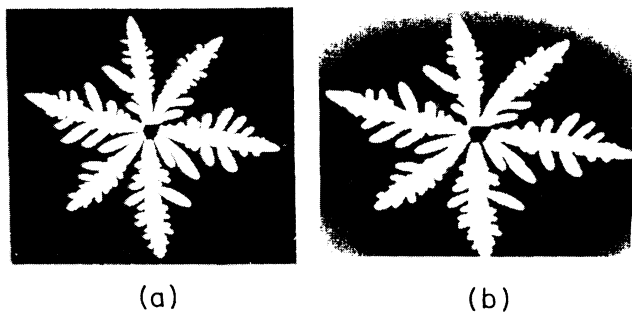


FIG. 1. (a) Photograph of a viscous-fingering pattern in an air-nematic liquid crystal system; (b) printout of its digitized image with a  $512 \times 512$  resolution.

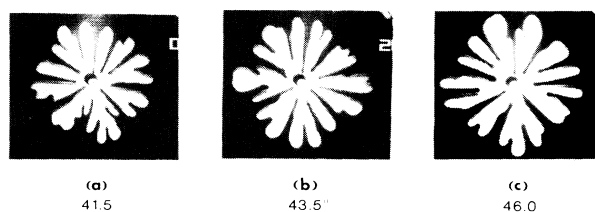


FIG. 2. Viscous fingers in an air-isotropic liquid crystal system.

was regulated by convective air flow and by a thermostatted substrate with water circulation. The sample temperature was varied between 50–25  $^\circ\text{C}$ . Patterns and their growth were recorded with a video camera in the isotropic, nematic, and the smectic  $A$  phases of 8CB. Signals from the video tape were digitized with  $512 \times 512$  resolution. The quality of the digitized images is illustrated in Fig. 1. Figure 1(a) shows the photograph of a pattern, while Fig. 1(b) is a printout of the digitized image on a laser printer with a different aspect ratio. Data analysis was carried out on microcomputers.

### RESULTS AND DISCUSSION

Patterns obtained at various temperatures are shown in Figs. 2–4. Pattern 2(a)–2(c) shows typical viscous fingering patterns with tip splitting, taken in the isotropic phase of 8CB.

In our stability analysis, we have assumed that the fluid is bounded by circular inner interface or radius  $R$  and a concentric outer interface of radius  $R_0$ . The assumption that the outer interface is a circle concentric with the inner one is clearly invalid for circular tips far

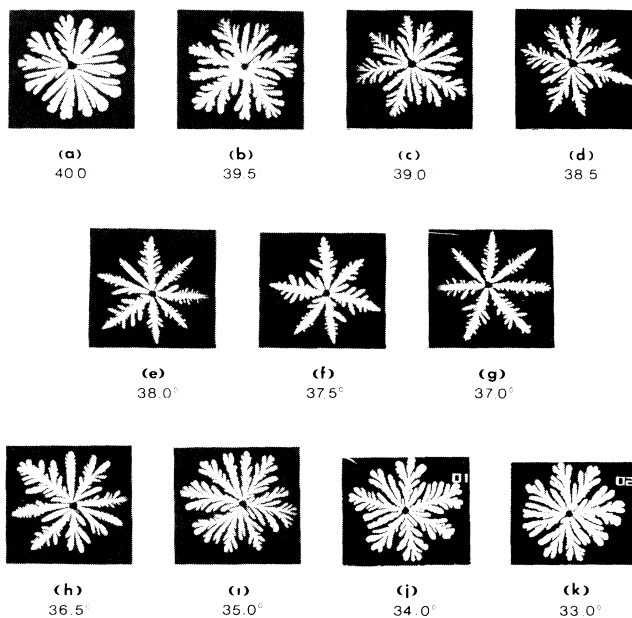


FIG. 3. Viscous fingers in an air-nematic liquid crystal system.

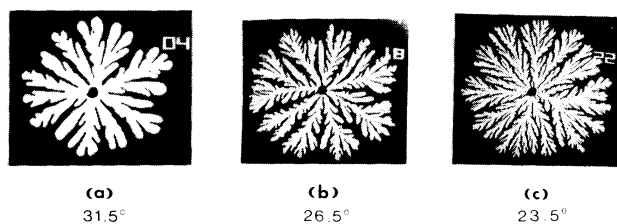


FIG. 4. Viscous fingers in an air-smectic liquid crystal system.

from the center of a circular cell, as well as for cells which are not circular and for cells which contain obstacles such as spacers. However, as suggested by Eq. (3), the pressure field near the center of the cell is not sensitively dependent on deviations of the outer interface from axial symmetry. We therefore assume that our stability analysis is valid for our cell if  $R \ll R_0$ , or if the pattern is small. The effects of deviations of the outer interface from cylindrical symmetry due to the cell shape and the presence of spacers may be seen in Figs. 2(a)–(c).

The wave number of the fastest growing mode  $m^*$  given in Eq. (6) can be approximated as being temperature independent, as the only material constant entering Eq. (6) is the surface tension which has a very weak temperature dependence. The isotropic viscosity scales the velocity everywhere and has no effect on the stability. Consequently, one does not expect any change of the characteristic finger thickness of the pattern at different temperatures in the isotropic phase.

Figures 3(a)–3(k) show patterns taken in the nematic phase of 8CB. Below  $T_{NI}$  (which is a first-order structural phase transition) the bulk properties of the system become anisotropic and the fluid flow created by the injection of the air causes the director to be radially aligned. In the vicinity of  $T_{NI}$  the anisotropy is too small to significantly affect the patterns. Figures 3(a) and 3(b) resemble the isotropic behavior shown in Figs. 2(a)–2(c). Decreasing the temperature causes the anisotropy to increase, and some tips grow stable [see Figs. 3(c) and 3(d)], indicating a morphological phase transition. The flow alignment gives rise to different viscosity coefficients in the radial and tangential directions. We have examined analytically the time evolution of a circular tip in a liquid crystal with viscosity  $\mu_r$  in the radial and  $\mu_t$  in the tangential direction. It is straightforward to show<sup>18</sup> that the radius of curvature of the tip will not increase if  $\mu_t/\mu_r \gtrsim 2$ . We claim, therefore, that the tip becomes stabilized in the nematic phase by the viscosity anisotropy, and the onset of dendritic regime occurs at the temperature where  $\mu_t/\mu_r \approx 2$ .

Figures 3(e)–3(g) show dendritic structures growing with stable tips in a well-defined temperature region in the middle of the nematic range. Another morphological phase transition occurs around 36.5°C [see Fig. 3(h)] where the dendritic growth is replaced by the tip-splitting regime again, resulting in a reentrant morphological phase change as a function of temperature.

For a typical nematic, the temperature dependence of

$\alpha_2$  and  $\alpha_3$  results in a decreasing  $\Theta_0$  with decreasing temperature, showing a typical value of 15–20° below  $T_{NI}$  and decreasing gradually to about 5° before the sample crystallizes.<sup>15</sup> However, if the liquid crystal has a low-temperature smectic phase below the nematic, which is the case for 8CB, then  $\alpha_3$  increases towards  $T_{NA}$  and still in the nematic phase changes from small negative to small positive values while  $\alpha_2$  remains necessarily negative for the system of rodlike molecules. When  $\alpha_3$  becomes positive, Eq. (7) will not allow a zero torque for a nonzero velocity gradient. Consequently, no equilibrium angle  $\Theta_0$  can be obtained. The flow alignment vanishes and there is a hydrodynamic torque acting on the molecules for any angle between  $\hat{n}$  and  $\vec{V}$ , resulting in a nonaligned, random distribution of the director and, consequently, an isotropic average viscosity in the sample.

Further cooling results in a further increase of  $\alpha_3$  as far as the nematic-smectic  $A$  transition where  $\alpha_3$  diverges. This is due to the layered structure of the smectic phase.  $\alpha_3$  is a viscosity coefficient determining the torque contribution for  $\hat{n}$  parallel to  $\vec{V}$  [see Eq. (7)], in the case of a smectic this means that layers are perpendicular to the flow direction. For flow to occur, molecules have to move from one layer to another and overcome a potential barrier associated with the layers, leading to diverging values of  $\alpha_3$ .

In our experiment with 8CB,  $\Theta_0$  has a value of 15° just below  $T_{NI}$ ,<sup>19</sup> and  $\mu_r$ , the effective viscosity in the radial direction, is higher than the viscosity for the case when the director is parallel to the velocity or the velocity gradient. The viscosity anisotropy itself is small at these high temperatures, consequently there is very little difference in the effective viscosities for flow in different directions ( $\mu_r \approx \mu_t$ ). With decreasing temperature two effects occur: the viscosity anisotropy of the liquid crystal increases and  $\Theta_0$  decreases. Both effects increase the difference between the effective viscosities for flow in the radial and tangential directions. At  $T \approx 38.5^\circ\text{C}$  the effective viscosity ratio  $\mu_t/\mu_r$  reaches the value of 2, and this results in stabilization of the tips and gives rise to stable dendritic structures [Figs. 3(c)–3(g)]. The most stable tips are obtained when  $\Theta_0$  reaches zero, which occurs around 37.5°C. This alignment corresponds to the maximum effective viscosity difference in the radial and tangential directions. Further cooling increases the viscosity anisotropy of the system, but because the flow alignment vanishes it eliminates the difference between the flow regimes in different directions. This stops the stable tip growth at this temperature still well in the nematic range [see Figs. 3(h)–3(k)], and the isotropic or tip-splitting regime reenters.

Figures 4(a)–4(c) show viscous fingers growing in the smectic  $A$  phase of 8CB. Patterns are characterized by tip splitting and belong to the dense-branching morphology. The characteristic finger thickness decreases with decreasing temperature.

There was no surface treatment used when preparing the sample, but 8CB exhibited a spontaneous homeotropic alignment, with the director perpendicular to the

TABLE I. Pattern exponents  $D_R$  and  $D_N$  and compactness parameter  $A$  at different temperatures.

$T$ (°C)	Phase	$D_R$	$A$	$D_N$
50	$I$	2.08	4.6 ± 0.2	1.30 ± 0.05
42		1.94 ± 0.08		
38.5	$N$	2.04	3.40	1.19
37.0		1.96 ± 0.08	3.40 ± 0.05	1.15 ± 0.05
36.0		1.98	3.00	1.21
31.5	$S_A$	1.98 ± 0.08	4.2 ± 0.2	1.03 ± 0.05

glass plates of the cell. This homeotropic alignment was destroyed by the flow in the nematic phase, creating a radial director configuration. When preparing the smectic phase, the sample was cooled undisturbed from the nematic, and it preserved the homeotropic alignment.

When the nematic–smectic  $A$  transition occurs and  $\alpha_3$  diverges, there is no flow parallel to the director. The smectic structure has a low viscosity if  $\hat{n}$  is perpendicular to  $\vec{V}$ , which, in the case of a radial flow, corresponds to a geometry where the planes of equal velocities are parallel with the smectic layers. Since a smectic  $A$  layer is a two-dimensional liquid (with no long-range positional order), there is no anisotropy in the flow in this plane. We again observe tip-splitting patterns in this case [Figs. 4(a)–4(c)].

Quantitative analysis of the digitized viscous fingering patterns and their time evolution has been carried out using two methods.

(1) The patterns obtained were recorded on video-cassette. Frames corresponding to successive stages of growth were digitized. For each frame, the radius of gyration  $R_g = \langle r_i^2 \rangle^{1/2}$ , where  $r_i$  is the distance of the  $i$ th pixel in the pattern from the center, and the mass  $M$  (area) of each pattern was calculated. Assuming that

$$M = AR_g^{D_R},$$

where  $A$  is a constant which gives a measure of the extent to which the pattern is space filling, we have plotted  $\log M$  versus  $\log R_g$ . The slope of the resulting straight lines gives the exponent  $D_R$ . Our data over a range greater than one decade is linear with a correlation coefficient greater than 0.999 65. The value of  $D_R$  obtained for all phases and temperatures is  $2.00 \pm 0.08$ ; thus for this case the Hausdorff dimension is the same as the Euclidean dimension and the structure is nonfractal. This nonfractal behavior agrees with previous observations<sup>4</sup> but differs from results of simulations.<sup>20</sup>

(2) We have calculated the number of surface points  $N_s$  on the perimeter of each pattern. The perimeter consists of pixels in the fingering pattern which are in edge contact with pixels outside the pattern. Assuming that

$$M = BN_s^{D_N},$$

where  $B$  is a constant, we have plotted  $\log M$  versus

$\log N_s$ . The slope of the resulting straight lines gives the exponent  $D_N$ . For nonfractal behavior, one would expect  $D_N$  to be 2. The calculated values for  $D_N$  are consistently less than 2, as indicated in Table I. The range of the data and the linearity are as given above.

Neither of the exponents indicate the morphological transitions clearly. The value of  $A$ , however, is significantly less in the dendritic regime than in the tip-splitting region, indicating that the dendritic morphology is less space filling than the dense-branching ones. (For a space-filling circular disk,  $A = 2\pi$ .) The value of  $A$  may be useful therefore to indicate transitions between these morphologies.

## CONCLUSIONS

We have studied viscous fingering patterns in the liquid crystal 8CB. Morphological transitions from dense branching to dendritic to dense branching were observed as a function of temperature in the nematic phase. We have analyzed the dense-branching patterns both in the isotropic and nematic phases, and we find that the pattern area is nonfractal, while the perimeter is fractal. We have shown elsewhere<sup>10</sup> that the predictions of linear stability analysis are in good agreement with experiment. We claim that a critical anisotropy in the viscosity is necessary for the stabilization of the tips of the viscous fingers and hence for the occurrence of a dendritic pattern. This critical anisotropy is achieved by flow alignment of the liquid crystal at low temperatures. As the temperature is lowered further, the flow alignment disappears due to the change of sign of one of the Leslie viscosity coefficients as the nematic–smectic  $A$  transition is approached from above. The ratio between the pattern area and the square of the radius of gyration provides a measure of the extent to which the pattern is space filling, and thus provides qualitative evidence of the morphological transition.

## ACKNOWLEDGMENTS

One of us (P.P.-M.) is grateful for support from the Natural Sciences and Engineering Research Council of Canada. The authors are indebted to B. Frisken and J. Gleeson for their help with the manuscript.

- \*On leave from Central Research Institute for Physics, P.O. Box 49, H-1525, Budapest, Hungary.
- †Present address: Liquid Crystal Institute, Kent State University, Kent, OH 44242.
- ‡On leave from Institute of Theoretical Physics, Eötvös University, H-1088 Budapest, Hungary.
- <sup>1</sup>P. G. Saffmann and G. I. Taylor, Proc. R. Soc. London, Ser. A **245**, 312 (1958).
- <sup>2</sup>J. Nittmann, G. Daccord, and H. E. Stanley, in *Fractals in Physics*, edited by L. Pietronero and E. Tosatti (Elsevier, New York, 1986), p. 193.
- <sup>3</sup>J. Nittmann, G. Daccord, and H. E. Stanley, Nature **314**, 141 (1985).
- <sup>4</sup>E. Ben-Jacob, G. Deutscher, P. Garik, N. D. Goldenfeld, and Y. Lareah, Phys. Rev. Lett. **57**, 1903 (1986).
- <sup>5</sup>J. Nittman and H. E. Stanley, Nature **321**, 663 (1986).
- <sup>6</sup>E. Ben-Jacob, R. Godbey, N. D. Goldenfeld, J. Koplik, H. Levine, T. Mueller, and L. M. Sander, Phys. Rev. Lett. **55**, 1315 (1985).
- <sup>7</sup>A. Buka, J. Kertesz, and T. Vicsek, Nature **323**, 424 (1986).
- <sup>8</sup>L. Paterson, J. Fluid Mech. **113**, 513 (1981).
- <sup>9</sup>H. Lamb, *Hydrodynamics* (Cambridge University Press, London, 1932), p. 581.
- <sup>10</sup>A. Buka and P. Palfy-Muhoray, Phys. Rev. A **36**, 1527 (1987).
- <sup>11</sup>C. W. Park and G. M. Homsy, J. Fluid Mech. **139**, 291 (1984).
- <sup>12</sup>R. L. Chuoke, P. van Meurs, and C. van der Poel, Pet. Trans. AIME **216**, 188 (1959).
- <sup>13</sup>W. W. Mullins and R. F. Sekerka, J. Appl. Phys. **34**, 323 (1963).
- <sup>14</sup>J. L. Ericksen, Mol. Cryst. Liq. Cryst. **7**, 153 (1969).
- <sup>15</sup>F. H. Leslie, Arch. Ration. Mech. Anal. **28**, 165 (1968).
- <sup>16</sup>E. Dubois-Violette, G. Durand, E. Guyon, P. Manneville, P. Pieranski, *Liquid Crystals* (Academic, New York, 1978), Suppl. 14, p. 147.
- <sup>17</sup>C. Gahwiller, Phys. Rev. Lett. **28**, 1554 (1972).
- <sup>18</sup>P. Palfy-Muhoray, A. Buka, and M. Plischke (unpublished).
- <sup>19</sup>W. W. Beens and W. H. de Jeu, J. Chem. Phys. **82**, 3841 (1985).
- <sup>20</sup>L. M. Sander, P. Ramanlal, and E. Ben-Jacob, Phys. Rev. A **32**, 3160 (1985).

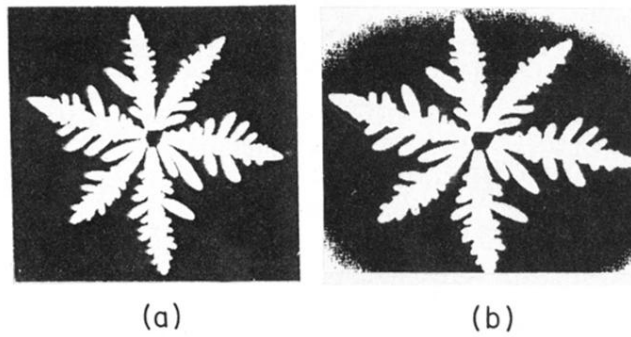


FIG. 1. (a) Photograph of a viscous-fingering pattern in an air-nematic liquid crystal system; (b) printout of its digitized image with a  $512 \times 512$  resolution.

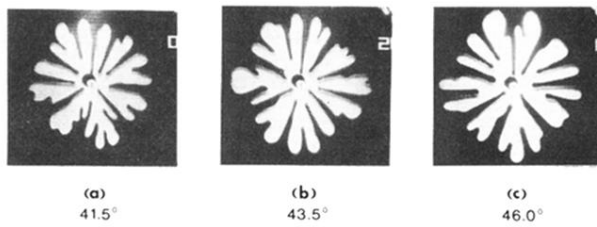


FIG. 2. Viscous fingers in an air–isotropic liquid crystal system.

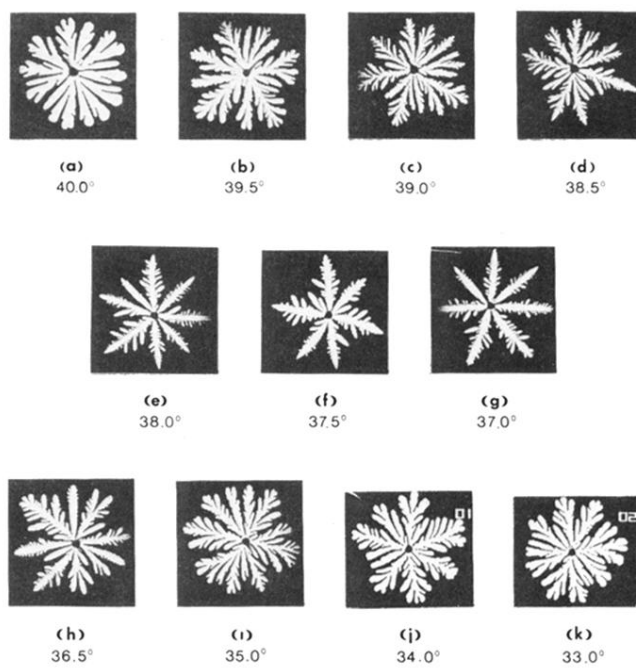


FIG. 3. Viscous fingers in an air–nematic liquid crystal system.

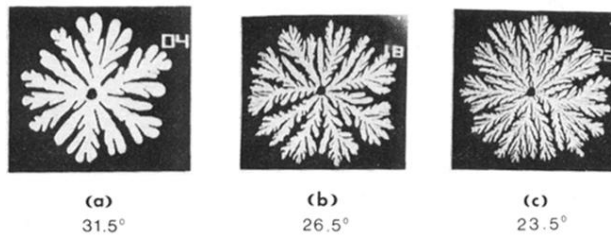


FIG. 4. Viscous fingers in an air-smectic liquid crystal system.